International Journal of Thermal Sciences 124 (2018) 399–406

Contents lists available at ScienceDirect

International Journal of Thermal Sciences

journal homepage: www.elsevier.com/locate/ijts

Performance analysis and multi-objective optimization of a Stirling engine based on MOPSOCD

Dongdong Dai, Fang Yuan, Rui Long, Zhichun Liu, Wei Liu*

School of Energy and Power Engineering, Huazhong University of Science and Technology, Wuhan 430074, PR China

ARTICLE INFO

Keywords:
Stirling engine
Finite time thermodynamics
Multi-objective optimization
Particle swarm optimization algorithm using crowding distance

ABSTRACT

A Stirling engine displays an aptitude for utilizing sustainable energy (such as solar energy) and exhibits the same theoretical efficiency as that of a Carnot cycle. However, the actual efficiency of a Stirling engine is far from the ideal Carnot efficiency due to irreversibilities. Models proposed in previous studies that focused on the imperfect regenerative process are crude and require improvements. In this study, finite time thermodynamics is employed to construct a refined model that considers the finite rate of heat transfer, conductive thermal bridging loss, and regenerative loss that is supplied by the heat source. Based on the model, three objective functions including power, efficiency, and ecological coefficient of performance (ECOP) of a Stirling engine are simultaneously optimized for maximization. A multi-objective optimization method based on a multi-objective particle swarm optimization algorithm using crowding distance (MOPSOCD) is employed to optimize the Stirling engine for the first time. Solutions obtained using the MOPSOCD comprise the Pareto set. The optimal solution is then selected using the technique for order of preference by similarity to ideal solution. The performance under the multi-objective optimization is compared with those of single-objective optimization methods in terms of power, efficiency, and ECOP. The results reveal that MOPSOCD exhibits good coordination in terms of the power, efficiency, and ECOP of the Stirling engine and may serve as a promising guide for operating and designing Stirling engines.

1. Introduction

Currently, with the reduction in fossil energy and the increase in environment-related problems it is extremely important to search for a productive method to utilize renewable energy [1,2]. Stirling engines are attractive engines for the future as they exhibit low emission, high efficiency, low noise, and work with a relatively long lifetime. Stirling engines display superiority in micro-cogeneration applications, renewable energy utilization, space power system, and low-grade heat recovery [3–7].

In the early nineteenth century, Robert Stirling devised the Stirling engine in Scotland [8], and its practical virtue as a simple, dependable, and secure engine was acknowledged following its invention [9]. Tlili et al. [10] constructed an irreversible Stirling model and researched the effect of regenerative efficiency and dead volume. Based on the Direct Method and the first law of thermodynamics, Costea and Petrescu [11,12] analyzed the process of a Stirling engine with finite speed. Curzon and Ahlborn [13] studied a Carnot engine with finite time. Following this, finite time thermodynamics (FTT) is applied in several engines including Stirling engines. Blank et al. [14] considered the irreversibility in the external heat transfer processes and analyzed an endoreversible Stirling engine with FFT and obtained the efficiency at maximum power. Senft [9] developed a mathematical model of Stirling engines with internal heat losses, mechanical friction losses, and limited heat transfer. Chen et al. [15] considered the limited heat transfer and regenerative losses and modeled and investigated the performance of a combined system that consisted of a Stirling engine and a solar collector. Wu et al. [16] investigated the optimal performance of a Stirling engine with a finite-speed effect in the regenerating processes and finite heat transfer in isothermal processes. Kaushik et al. [17–19] used the FTT method to develop a Stirling heat engine and pump model that is subject to a finite heat capacitance rate of working substance, the heat leak between two reservoirs, and regenerative losses. Ahmadi et al. [20] studied the effect of design parameters on a Stirling system model that considered finite-rate heat transfer, regenerative heat loss, conductive thermal bridging loss, and finite regeneration process time.

Several studies examined the optimization of Stirling cycle engines. Li et al. [21] optimized the power of a solar-driven Stirling cycle model and derived the corresponding efficiency. Tyagi et al. [22] optimized the thermo-economic function of a Stirling heat pump and indicated

* Corresponding author.
E-mail address: W_Liu@hust.edu.cn (W. Liu).

http://dx.doi.org/10.1016/j.ijthermalsci.2017.10.030
Received 6 June 2017; Received in revised form 25 October 2017; Accepted 25 October 2017

that regenerative effectiveness significantly affected the performance of a cycle. An "ecological" standard for the optimum operation of finite-time heat engines [23] involves maximizing an equation that represents the optimal trade-off between power and the product of the temperature of the heat sink and entropy production. Yan [24] pointed out that replacing the temperature of the heat sink with ambient temperature is more suitable. Long et al. [25] maximized the ecological function for general heat engines and obtained the corresponding efficiency and its bounds. He et al. [26], Tyagi et al. [27], and Ahmadi et al. [28–30] optimized different cycles under the ecological standard proposed by Yan. Long et al. [31,32] optimized the performance of the Stirling-like thermally regenerative electrochemical cycle (TREC) under the maximum power and ecological criteria. The ecological coefficient of performance (ECOP), which is a positive ecological function proposed by Ust [33], is defined as the ratio of power output to the loss rate of availability, and Ahmadi et al., applied it to optimize an absorption heat pump [34]. Conflict can exist between objective functions of an engine, and thus multi-objective optimization was proposed to simultaneously optimize multiple criteria as opposed to single objective optimization. Sadatsakkak and Ahmadi et al. examined multi-objective optimization of different cycles for various operating circumstances [35–42]. Luo et al. [43] adopted an algorithm combined by adaptive simulated annealing and a genetic algorithm towards the performance optimization of Stirling engines. The multi-objective optimization method based on the second version of non-dominated sorting genetic algorithm (NSGA-II) was used by Ahmadi et al. [44–51] to perform studies on Stirling engines. Long et al. [52] conducted a multi-objective optimization of the Stirling -like TREC with maximum power output and maximum exergy efficiency as the objective functions simultaneously. Kennedy and Eberhart [53] proposed particle swarm optimization (PSO) with a faster convergence speed when compared with that of the genetic algorithm. Coello et al. [54] presented a multi-objectives particle swarm optimization algorithm (MOPSO) for multi-optimization. Duan et al. [55] applied MOPSO in a Stirling engine with the triple objectives of power, efficiency, and the irreversibility parameter. Nevertheless, the PSO algorithm can easily lapse into local convergence. In order to solve this, Raquel and Naval [56] presented a multi-objective particle swarm optimization algorithm using crowding distance (MOPSOCD) that exhibits a better convergence and capability to maintain diversity.

With respect to evaluating the performance of Stirling engine, several studies focused on the four common processes in a Stirling cycle as follows: expansion, compression, and two regeneration processes. Few efforts focused on studying the complementary regenerative heat loss. In order to resolve this, we propose a modified Stirling engine model with FTT. Furthermore, three key criteria, namely power, efficiency, and ECOP of the model are obtained and simultaneously optimized by MOPSOCD.

2. Theoretical model

The Stirling cycle consists of two isothermal branches and two isochoric regenerating branches. As shown in Fig. 1, the Stirling engine absorbs heat from a heat source with constant temperature T_H and releases heat to a heat sink with a constant temperature T_C in the model. It is necessary for the four branches of the actual Stirling engine to proceed within a finite time, and thus, the heat transfer between the external heat reservoirs and working substance occurs with a finite temperature difference. Because of imperfect regeneration, the outlet states of working substance in the absorbing and releasing heat processes inside the regenerator are at 3′ as opposed to 3 and 1′ as opposed to 1, respectively. In order to circulate the working substance as a Stirling cycle, it is necessary to cool down the working substance to T_3 at a constant volume with heat removed to the external heat sink.

According to heat transfer theory, the rates of heat transfer out of and into the working substance are proportional to the temperature differences between the working substance and external heat reservoirs. Thus, we express the heat transfer during expansion and compression processes as follows:

$$Q_{3-4} = \alpha_h(T_H - T_h)t_{3-4} \tag{1}$$

and

$$Q_{1-2} = \alpha_l(T_l - T_L)t_{1-2} \tag{2}$$

respectively, where α_h denotes the thermal convection between working substance and heat source at temperature T_H, α_l denotes the thermal convection between working substance and heat sink at temperature T_L, and t_{3-4} and t_{1-2} denote durations of the two isothermal branches in processes 3–4 and 1–2, respectively.

Process 3–4 is an isothermal process, and thus heat released from a heat reservoir to working substance equals the work performed by the working substance as follows:

$$Q_{3-4} = nRT_h \ln\lambda \tag{3}$$

where n, R, and λ denote moles of the working substance, perfect gas constant, and volume compression ratio, respectively. With respect to the Stirling cycle, λ is defined as follows:

$$\frac{V_1}{V_2} = \frac{V_4}{V_3} = \lambda \tag{4}$$

Similarly, in process 1–2, the following expression is obtained:

$$Q_{1-2} = nRT_l \ln\lambda \tag{5}$$

In process 2–3, given the imperfect regenerative of the actual Stirling engine, the temperature of working substance are unable to reach T_3 but only reach $T_{3'}$ after the working substance absorbs heat from the regenerator. The imperfect regeneration coefficient of process 2–3 is denoted by μ_{2-3}, and the heat loss and heat transferred during this process are expressed as follows

$$Q_{3'-3} = \mu_{2-3}Q_{2-3} \tag{6}$$

$$Q_{2-3'} = Q_{2-3} - Q_{3'-3} = (1 - \mu_{2-3})Q_{2-3} \tag{7}$$

Similarly, we denote the imperfect regeneration coefficient of process 4–1 by μ_{4-1}, and this results in the following expression:

$$Q_{1'-1} = \mu_{4-1}Q_{4-1} \tag{8}$$

$$Q_{4-1'} = Q_{4-1} - Q_{1'-1} = (1 - \mu_{4-1})Q_{4-1} \tag{9}$$

The regenerative processes are isochoric, and thus heat exchanged in these processes is expressed as follows:

$$Q_{2-3} = Q_{4-1} = mc(T_h - T_l) \tag{10}$$

where c refers to the constant volume specific heat capacity of the working substance.

In order for a working substance to operate as a Stirling cycle, it is necessary to heat the working substance to T_3 prior to the expansion process and cool it down to T_1 prior to the compression process. While dealing with regeneration loss in regenerative process 2–3, researchers assume that the regenerative loss is supplied by the external heat reservoir. Therefore, the actual heat released by heat reservoir is as follows:

$$Q_h = Q_{3-4} + Q_{3'-3} \tag{11}$$

The actual time required for the heat exchange is as follows:

$$t_{3'-4} = \frac{Q_{3-4} + Q_{3'-3}}{\alpha_h(T_H - T_h)} \tag{12}$$

According to Eqs. (1) and (12), the heat transfer during process 3′–3 is expressed as follows:

$$Q_{3'-3} = \alpha_h(T_H - T_h)t_{3'-3} \tag{13}$$

The above function indicates that the temperature of working substance remains constant at T_h during process 3′–3, and this conflicts

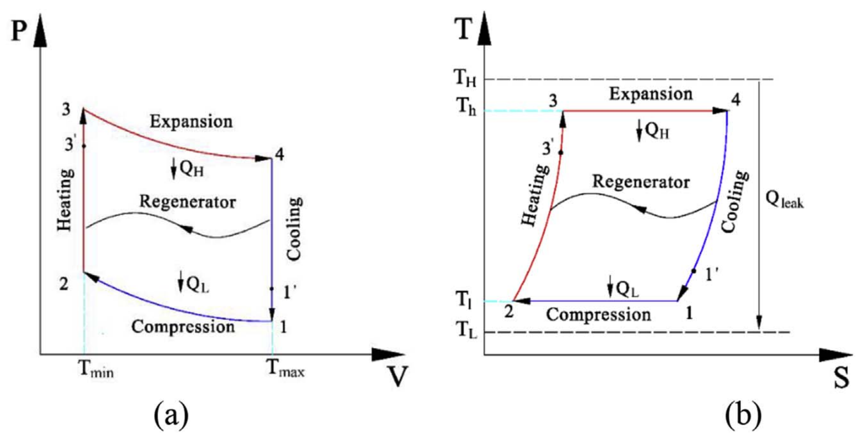

Fig. 1. *P-V* (a) and *T-S* (b) scheme of the Stirling engine.

with the fact that the temperature of working substance increases from $T_{3'}$ to T_3. In order to resolve this contradiction, we continue to consider the regenerative heat loss as replenished by heat reservoirs, albeit with the difference that the processes are isochoric as opposed to isothermal. We use variable T to represent the variable temperature of the working substance, and the heat transfer during process 3′–3 is represented as follows:

$$dQ_{3'-3} = \alpha_h (T_H - T)dt \tag{14}$$

The conservation of energy in process 3′–3 is as follows:

$$dQ_{3'-3} = mcdT \tag{15}$$

Combining Eqs. (14) and (15), we can obtain the time required for process 3′–3 as follows:

$$t_{3'-3} = \frac{mc}{\alpha_h}\ln\left(\frac{T_H - T_{3'}}{T_H - T_3}\right) \tag{16}$$

Similarly, we obtain the time required for isochoric process 1′–1 as follows:

$$t_{1'-1} = \frac{mc}{\alpha_l}\ln\left(\frac{T_{1'} - T_L}{T_1 - T_L}\right) \tag{17}$$

Because of the finite-time effect in regenerating processes, we assume that the temperature of the working substance changes linearly over time when the regenerating processes proceed, and this is expressed as follows:

$$\frac{dT}{dt} = \pm k_i \qquad (i = 1,2) \tag{18}$$

where k_i denotes a positive constant. In the regenerative heating process, we use the sign “+” and $i = 1$ while we use the sign “−” and $i = 2$ in the regenerative cooling process. Therefore, the duration of regenerative processes is expressed as follows:

$$t_{2-3'} = \frac{T_{3'} - T_2}{k_1} \tag{19}$$

$$t_{4-1'} = \frac{T_4 - T_{1'}}{k_2} \tag{20}$$

Based on the above equations, we obtain the duration of the Stirling cycle as follows:

$$\begin{aligned}\tau &= t_{1-2} + t_{2-3'} + t_{3'-3} + t_{3-4} + t_{4-1'} + t_{1'-1}\\ &= \left(\frac{1-\mu_{2-3}}{k_1} + \frac{1-\mu_{4-1}}{k_2}\right)(T_h - T_l) + \frac{cm}{\alpha_h}\ln\frac{T_H - \mu_{2-3}T_l - (1-\mu_{2-3})T_h}{T_H - T_h}\\ &\quad + \frac{cm}{\alpha_l}\ln\frac{\mu_{4-1}T_h + (1-\mu_{4-1})T_l - T_L}{T_l - T_L} + \frac{nRT_h\ln\lambda}{\alpha_h(T_H - T_h)} + \frac{nRT_l\ln\lambda}{\alpha_l(T_l - T_L)}\end{aligned} \tag{21}$$

and the heat leakage proportional to the temperature difference between heat source and heat sink can be expressed as

$$Q_{leak} = \alpha_{leak}(T_H - T_L)\tau \tag{22}$$

where α_{leak} denotes the thermal leak coefficient between the heat source and heat sink. Therefore, the actual amounts of heat released from and to the external heat reservoirs in a cycle are as follows, respectively:

$$Q_H = Q_{3'-3} + Q_{3-4} + Q_{leak} \tag{23}$$

$$Q_L = Q_{1'-1} + Q_{1-2} + Q_{leak} \tag{24}$$

The entropy generation rate of this cycle is obtained as follows [57]:

$$\dot{\sigma} = \frac{\frac{Q_L}{T_L} - \frac{Q_H}{T_H}}{\tau} \tag{25}$$

The above equations are used to express the power, efficiency, and ECOP of the Stirling engine as follows:

$$P = \frac{nR(T_h - T_l)\ln\lambda}{\tau} \tag{26}$$

$$\eta = \frac{P}{Q_H} = \frac{nR(T_h - T_l)\ln\lambda}{\alpha_{leak}(T_H - T_L)\tau + \mu_{2-3}cm(T_h - T_l) + nRT_h\ln\lambda} \tag{27}$$

$$\begin{aligned}ECOP &= \frac{P}{T_0\dot{\sigma}}\\ &= nR\ln\lambda(T_h - T_l)T_0^{-1}\left(\begin{aligned}&\frac{\alpha_{leak}(T_H - T_L)\tau + \mu_{4-1}cm(T_h - T_l) + nRT_l\ln\lambda}{T_L}\\ &-\frac{\alpha_{leak}(T_H - T_L)\tau + \mu_{2-3}cm(T_h - T_l) + nRT_h\ln\lambda}{T_H}\end{aligned}\right)^{-1}\end{aligned} \tag{28}$$

3. Optimization with MOPSOCD

With respect to the optimization of an engine, the objective functions may conflict with each other. This is resolved by applying multi-objective optimization that yields the best solution by counterpoising the incompatible objective function.

Among swarm intelligence optimization algorithms, PSO exhibits the characteristic of fast convergence in single-objective optimization problems. In the PSO algorithm, the individuals that are considered as particles are those that lack volume and quality, fly in the search space at a certain speed, and dynamically adjust the speed based on the integrated analysis of the individual and collective flight experience over generations.

The PSO algorithm was extended to deal with multi-objective optimizations. Coello [54] compared the capacity of several evolutionary algorithms in solving multi-objective optimization problems and concluded that the MOPSO requires less execution time and exhibits better convergence to the true Pareto set when compared to NSGA- II. Carlo extended MOPSO and included the selection of leaders from an external archive by using a crowding distance mechanism to aid in the retention of the diversity of nondominated solutions.

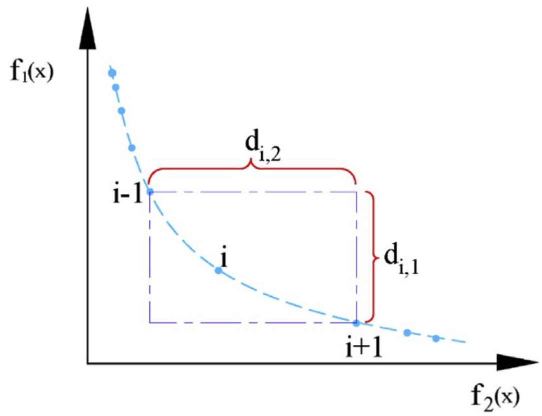

Fig. 2. Crowding distance in the Pareto frontier.

Similar to the nondominated solutions in NSGA-II, the crowding distance adopted in MOPSOCD is obtained by measuring the perimeter of the cube that is formed by the neighboring individuals as vertices. Prior to calculating the crowding distance, it is necessary to sort the set of solutions in ascending order by the function value. As shown in Fig. 2, with respect to particle i, the mean distance of its two adjacent particles in the Pareto frontier, namely particles $i-1$ and $i+1$, is defined as its crowding distance as follows:

$$d_i = \frac{d_{i,1} + d_{i,2}}{2} \tag{31}$$

A higher crowding distance indicates a lower density of the individual distribution and higher diversity of the solution. Conversely, a lower crowding distance denotes higher density of the individual distribution and a lower diversity of the solution. The structure of MOPSOCD that is applied here is illustrated in Fig. 3.

In this study, triple objective functions including power, efficiency, and ECOP of Stirling engine that are denoted by (26), (27), and (28), respectively, are optimized for simultaneous maximization. We select Helium as the working substance. Imperfect regeneration coefficients, temperature change rates in the regeneration processes, coefficients of heat transfer, environment temperature, and thermal leak coefficient are selected as the known parameters. The parameters for optimization include temperatures of the heat source, heat sink, and working substance in the expansion and compression chambers. In order to ensure consistency with previous studies [16], the specifications are listed in Table 1.

Four decision variables, namely T_h, T_l, T_H, and T_L that denote the temperature of the working substance in the expansion chamber,

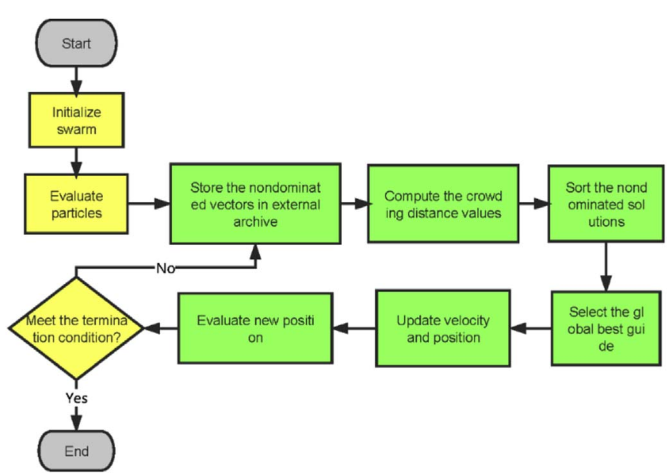

Fig. 3. The flow chart of MOPSOCD.

Table 1
Specifications of the Stirling engine.

Specifications	Values
Working substance	Helium
Moles of working substance n	1 mol
Mass of working substance m	4 g
Specific heat capacity c_v	3.214 J/(g·K)
Ideal gas constant R	8.314 J/(mol·K)
Imperfect regeneration coefficient μ_{2-3}	0.3
Imperfect regeneration coefficient μ_{4-1}	0.2
Temperature change rate k_1	5000 K/s
Temperature change rate k_2	5000 K/s
Coefficient of heat transfer α_h	1000 W/(K·s)
Coefficient of heat transfer α_l	1000 W/(K·s)
Environment temperature T_0	300 K
Conductive thermal bridge loss coefficient α_{leak}	12 W/(K·s)

temperature of the working substance in the compression chamber, temperature of the heat source, and temperature of the sink, respectively, follow the constraints given below:

$$600 \le T_h \le 1000\ \mathrm{K} \tag{32}$$

$$300 \le T_l \le 600\ \mathrm{K} \tag{33}$$

$$1000 \le T_H \le 1200\ \mathrm{K} \tag{34}$$

$$280 \le T_L \le 300\ \mathrm{K} \tag{35}$$

In the multi-objective problem, a Pareto set is derived, and a procedure to select the final optimal result through decision making is required. In this study, the technique for order preference by similarity to an ideal solution (TOPSIS) is adopted to obtain a decision.

4. Results and discussion

Heat transfer coefficients heat transfer between the working substance and heat reservoirs, α_h and α_l, are important parameters in the Stirling engine design, whose effects on the output power, thermal efficiency, and ECOP of the Stirling engine are depicted in Fig. 4. It can be observed that as the heat transfer coefficients, α_h or α_l, increases, both the efficiency and power increase substantially at first, then approach constant values, while the ECOP remains constant. Therefore, large heat transfer coefficients between the working substance and heat reservoirs are required to improve the thermal efficiency and output power of the Stirling engine model. However, they present no influence on the ECOP of the Stirling engine model.

The effects of the conductive thermal bridge loss coefficient on the output power, thermal efficiency, and ECOP of the Stirling engine are

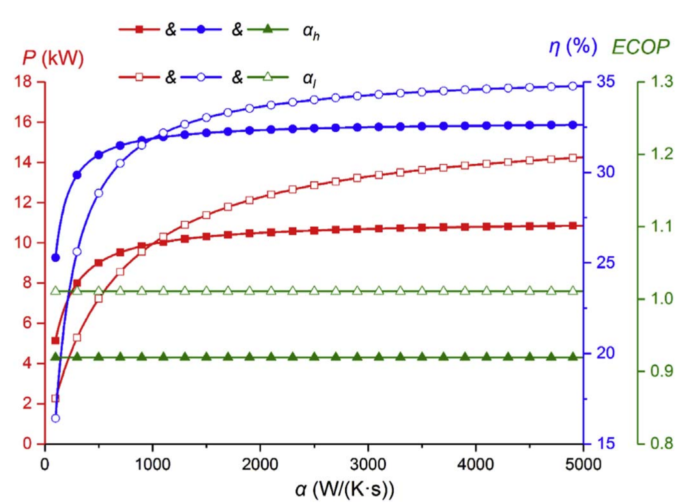

Fig. 4. Power, efficiency, and ECOP versus coefficients of heat transfer.

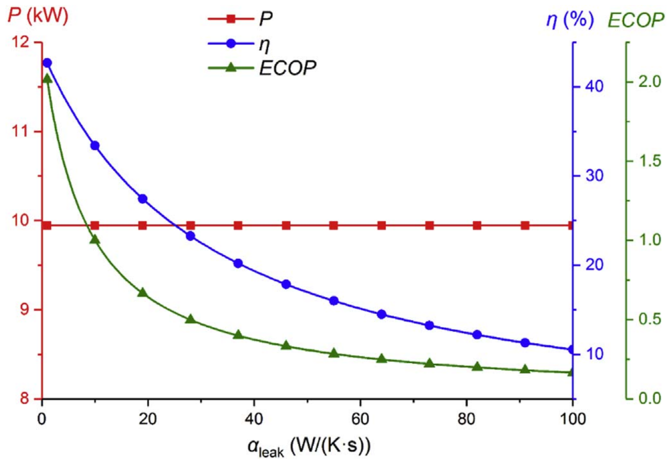

Fig. 5. Power, efficiency, and ECOP versus conductive thermal bridge loss coefficient.

depicted in Fig. 5. In Fig. 5, by increasing the conductive thermal bridge loss coefficient, both the thermal efficiency and ECOP decrease while the output power remains constant. Therefore, a small conductive thermal bridge loss coefficient is required to improve the thermal efficiency and ECOP of the Stirling engine model.

To coordinate the conflicting performance criteria, the thermal efficiency, output power, and ECOP of the Stirling engine are simultaneously maximized using the multi-objective optimization method that works based on the MOPSOCD algorithm. In this, the optimization process is conducted by objective functions as expressed in Eqs. (26)–(28). The decision variables (design parameters) of optimization include the temperatures of the working substance in expansion chamber and compression chamber and the temperatures of heat source and sink with constraints as stated in Eq. (32) − (35).

Fig. 6 shows the Pareto frontier in the proposed objectives' space that is obtained using MOPSOCD with the options specified in Table 1. In this figure, we observe the conflicting relationship that is evident among the triple objectives. With respect to the parameters given above, the ideal point should be located at the top-right-front, and this leads to the maximum efficiency, the highest power, and the highest ECOP. In contrast, the non-ideal point should be located at the bottom-left-back, and this leads to the lowest efficiency, the least power, and the least ECOP. The red balls represent the Pareto optimality derived by MOPSOCD. It is observed that the optimal solutions are located in 10.86 kW ≤ P ≤ 14.60 kW, 28.47% ≤ η ≤ 33.49% and 0.64 ≤ $ECOP$ ≤ 1.09. The green ball represents the final optimal point selected by

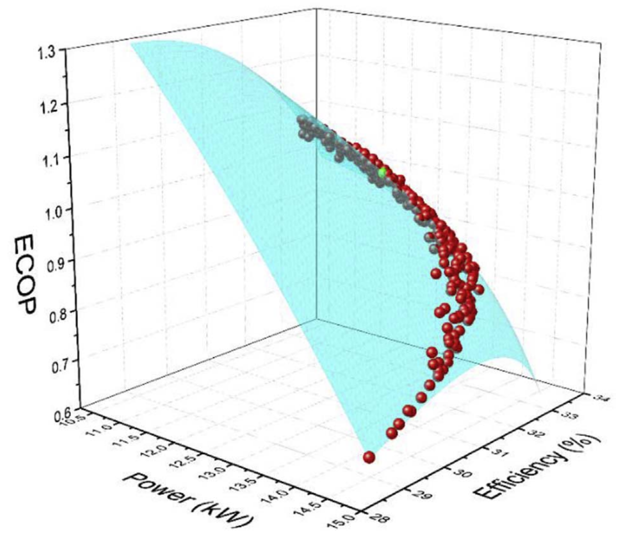

Fig. 7. Efficiency, power, and the ECOP Pareto frontier with the surface fit.

TOPSIS, and this is the ideal solution in coordination. The corresponding output power, thermal efficiency, and ECOP are 12.44 kW, 32.62%, and 1.02, respectively.

A compact way to determine the direct or indirect association of optimal data points of the model involves the use of surface fitting to promote the determination of intermediate values among reference points. As depicted in Fig. 7, we construct a surface to fit the Pareto frontier that results from MOPSOCD, and the fitted equation is expressed as follows:

$$ECOP = \frac{2.35\times 10 - 3.64\times P + 1.50\times\eta - 5.28\times 10^{-2}\times\eta^2 - 8.06\times 10^{-2}\times P\times\eta}{1 + 2.79\times P - 3.50\times 10^{-3}\times\eta - 1.31\times 10^{-2}\times P^2 + 1.27\times 10^{-2}\times\eta^2 - 1.17\times 10^{-1}\times P\times\eta} \tag{36}$$

This is applied to gain the ECOP for a given efficiency and power.

The Pareto frontiers for the dual-objective optimization (η-P, P-ECOP, ECOP-η) are depicted in Figs. 8 − 10.

Fig. 8 illustrates the Pareto optimal frontier for efficiency and power of the Stirling engine. It is observed that the power varies from 12.3 kW to 14.6 kW and the efficiency varies from 28.6% to 33.5%. It is also observed in Fig. 8 that the efficiency of Stirling engine decreases with an increase in power. This tendency results from a conflicting nature between maximizing thermal efficiency and output power of the

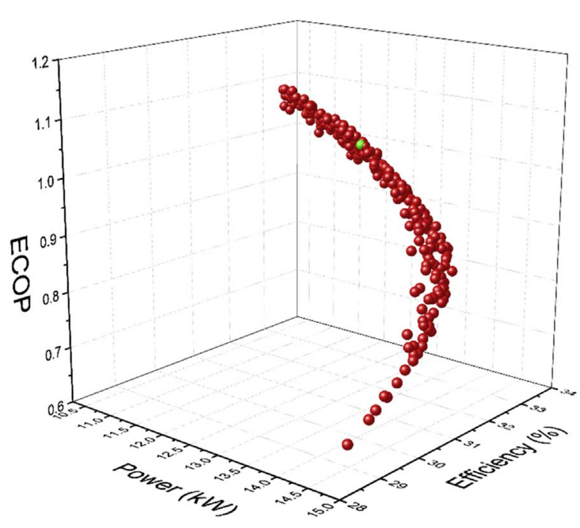

Fig. 6. Pareto optimal front in objective space.

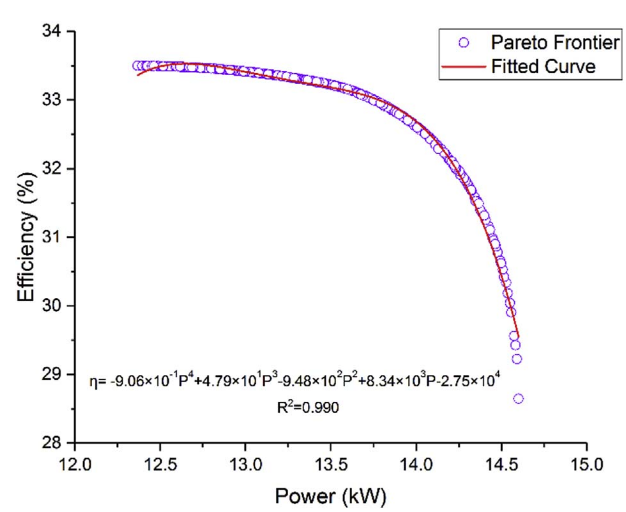

Fig. 8. Pareto optimal front in objective space (η-P).

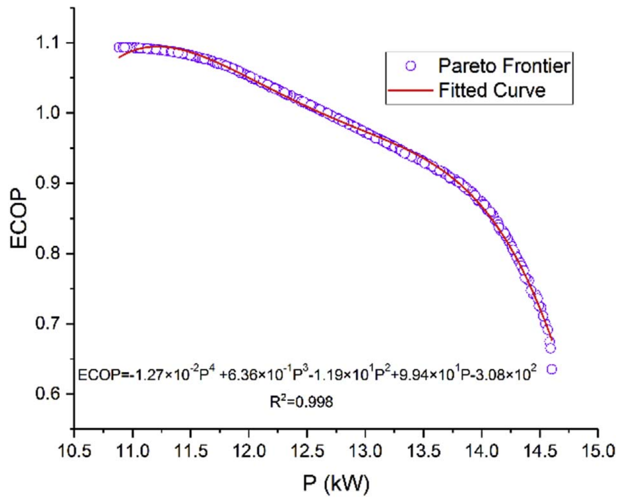

Fig. 9. Pareto optimal front in objective space (*P*-ECOP).

Stirling engine as shown in Eqs. (25) and (26). In order to aid the optimization of Stirling engine design, the curve fitting formula for efficiency and power is derived as follows:

$$\eta = -9.06\times10^{-1}P^4 + 4.79\times10^1P^3 - 9.48\times10^2P^2 + 8.34\times10^3P - 2.75\times10^4 \quad (37)$$

Fig. 9 illustrates the Pareto optimal frontier for power and ECOP of the Stirling engine. The power varies from 0.64 to 1.09, and the thermal efficiency varies from 10.9 kW to 14.6 kW. It is also observed in Fig. 9 that the power of Stirling engine decreases with an increase in ECOP. This tendency results from a conflict between maximizing output power and ECOP of the Stirling engine as expressed in Eqs. (25) and (27). In order to facilitate the optimization of the Stirling engine design, the curve fitting formula of power and ECOP is derived as follows:

$$P = -2.25\times10^1 ECOP^3 + 3.72\times10^1 ECOP^2 - 2.00\times10^1 ECOP + 1.81\times10^1 \quad (38)$$

Fig. 10 illustrates the Pareto optimal frontier for ECOP and efficiency of the Stirling engine. The power varies from 32.7% to 33.5%, and the thermal efficiency varies from 0.92 to 1.09. It is also observed from Fig. 10 that the ECOP of Stirling engine decreases with an increase in efficiency. This tendency results from a conflict between maximizing ECOP and thermal efficiency of the Stirling engine as shown in Eqs. (27) and (26). In order to facilitate the optimization of the Stirling engine design, the curve fitting formula of ECOP and efficiency is derived as

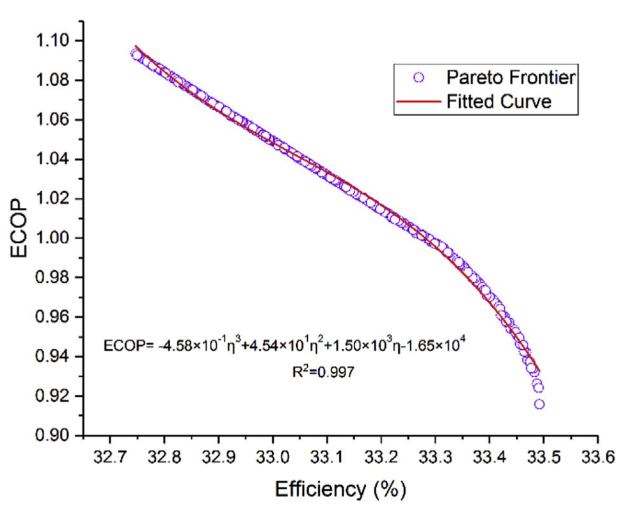

Fig. 10. Pareto optimal front in objective space (ECOP-η).

Table 2
Optimization results under different optimization methods.

Optimization algorithm	Objective			Variable			
	P [kW]	η [%]	$ECOP$	T_h [K]	T_l [K]	T_H [K]	T_L [K]
Maximum Power	14.60	28.47	0.64	874.3	455.4	1200.0	280.0
Maximum Efficiency	12.23	33.49	0.92	985.1	325.2	1119.2	280.0
Maximum ECOP	10.86	32.74	1.09	896.8	340.2	1000.0	300.0
MOPSOCD (TOPSIS)	12.44	32.62	1.02	917.0	362.3	1070.4	300

follows:

$$ECOP = -4.58\times10^{-1}\eta^3 + 4.54\times10^1\eta^2 + 1.50\times10^3\eta - 1.65\times10^4 \quad (39)$$

The results obtained by MOPSOCD and single objective optimizations are compared in Table 2 and Fig. 11 in detail. In Fig. 11, the light blue ball, green ball, and dark blue ball represent the states for single-objective optimizations based on maximum output power, thermal efficiency, and ECOP of the Stirling engine, respectively. The red ball represents the state optimized by MOPSOCD and selected by the TOPSIS decision making method. In Table 2, the values of three objective functions optimized by different methods and corresponding decision variables are listed for purposes of comparison. When compared with the optimal result obtained by the single-objective optimization of power, the optimal result under MOPSOCD was obtained as 14.79% lower in terms of power, but 14.58% and 59.38% higher in terms of efficiency and ECOP, respectively. With the exception of a significant increase in ECOP, the result obtained by MOPSOCD exhibited a slight advantage in terms of the amount of increase in efficiency than that of the reduction in power. When compared with the optimal result obtained by the single-objective optimization of efficiency, the result optimized by MOPSOCD and selected by TOPSIS was 1.72% and 10.87% better in terms of power and ECOP, respectively. The efficiency optimized by MOPSOCD was 2.60% lower than that derived by the single-objective optimization for efficiency. Nevertheless, the result obtained by proposed MOPSOCD is still competitive. It is slightly higher in efficiency, and it also led to a significant increase in ECOP. When compared with the optimal result obtained by the single-objective optimization of ECOP, the optimal result under MOPSOCD was 0.37% and 6.42% lower in terms of efficiency and ECOP, respectively, albeit 14.55% higher in terms of power. With a slight reduction in efficiency and ECOP, the optimal power under MOPSOCD was significantly higher than that derived by the single-objective optimization for ECOP. Thus, MOPSOCD leads to a more desirable design of the Stirling engine if it is compared with single objective optimization methods.

5. Conclusions

In the present study, a more realistic Stirling engine model with thermal resistance, conductive thermal bridging loss, and regenerative losses was established using FTT. Regeneration is an important part of a Stirling engine, and thus the analysis focused on nonnegligible regenerative losses. This is different from the FTT analysis on Stirling engines in extant studies as the complementary regenerative losses supplied by external heat reservoirs were considered in a more rational way, and corresponding time was individually evaluated. As a result, a more practical Stirling model was established and its output power, thermal efficiency, and ECOP functions were obtained.

Additionally, thermal efficiency, output power, and ECOP of the Stirling model were derived and simultaneously optimized for maximization. A multi-objective optimization method based on the MOPSOCD algorithm was employed in Stirling engine for the first time. Furthermore, TOPSIS was used in strategic decision-making to select the final optimal result of the Stirling engine. Moreover, we compared

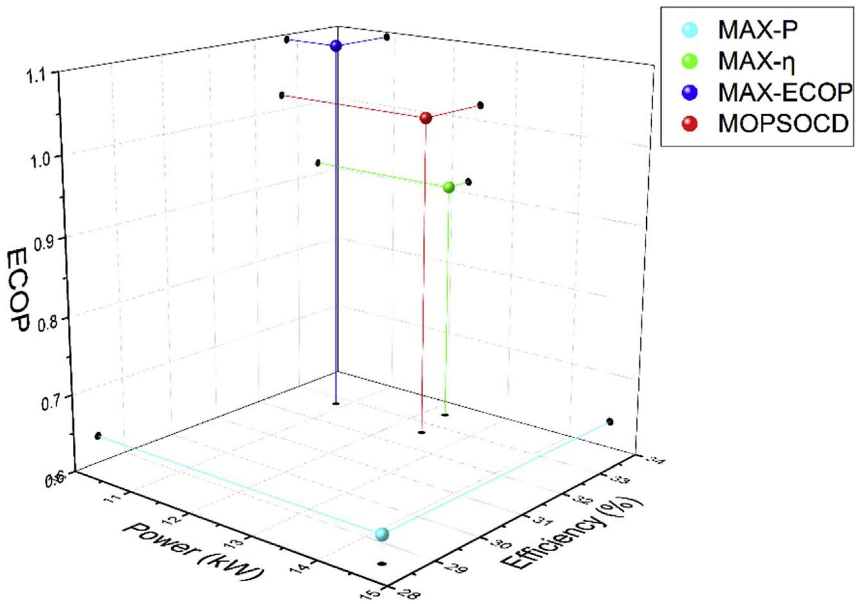

Fig. 11. Comparison of efficiency, power and ECOP under different optimization methods.

the solution obtained by MOPSOCD with those obtained by single-objective optimization method. The results revealed that the power, efficiency, and ECOP obtained under MOPSOCD exhibited moderate values indicating that the optimal result obtained by MOPSOCD adequately harmonizes performance of Stirling engines. The findings indicate that the MOPSOCD provides an alternative method for Stirling engine design and its optimal result exhibits a desirable performance when compared with that of the single-objective optimization approach.

Acknowledgments

We acknowledge the support received from the National Natural Science Foundation of China (51736004, 51706076).

Nomenclature

c	constant volume specific heat capacity, [J/(g·K)]
d	distance, [—]
ECOP	ecological coefficient of performance, [—]
i	natural number, [—]
k_1, k_2	temperature change rates in regenerative processes, [K/s]
m	mass of working substance, [g]
n	mole of working substance, [—]
P	power, [W]
Q	heat, [J]
R	perfect gas constant, [—]
S	entropy, [J/K]
t	time, [s]
T	temperature, [K]
V	volume, [m^3]

Greek symbols

α	thermal convection, [W/K]
λ	volume compression ratio, [—]
$\dot{\sigma}$	entropy generation rate, [J/(K·s)]
η	efficiency, [—]
τ	cyclic duration, [s]
μ	imperfect regeneration coefficient, [—]

Subscripts

h	expansion process
H	heat source
l	compression process
L	heat sink
leak	thermal leak
1, 1′, 2, 3, 3′, 4	state points

References

[1] R. Long, Y.J. Bao, X.M. Huang, W. Liu, Exergy analysis and working fluid selection of organic Rankine cycle for low grade waste heat recovery, Energy 73 (0) (2014) 475–483.
[2] R. Long, B. Li, Z. Liu, W. Liu, Hybrid membrane distillation-reverse electrodialysis electricity generation system to harvest low-grade thermal energy, J Membr Sci 525 (2017) 107–115.
[3] K. Wang, S.R. Sanders, S. Dubey, F.H. Choo, F. Duan, Stirling cycle engines for recovering low and moderate temperature heat: a review, Renew Sustain Energy Rev 62 (2016) 89–108.
[4] S.Q. Fan, M.H. Li, S.Z. Li, T. Zhou, Y.P. Hu, S. Wu, Thermodynamic analysis and optimization of a Stirling cycle for lunar surface nuclear power system, Appl Therm Eng 111 (2017) 60–67.
[5] H. Damirchi, G. Najafi, S. Alizadehnia, R. Mamat, N.A.C. Sidik, W.H. Azmi, et al., Micro Combined Heat and Power to provide heat and electrical power using biomass and Gamma-type Stirling engine, Appl Therm Eng 103 (2016) 1460–1469.
[6] I. Barreno, S.C. Costa, M. Cordon, M. Tutar, I. Urrutibeascoa, X. Gomez, et al., Numerical correlation for the pressure drop in Stirling engine heat exchangers, Int J Therm Sci 97 (2015) 68–81.
[7] Z.G. Li, Y. Haramura, D.W. Tang, C.H. Guo, Analysis on the heat transfer characteristics of a micro-channel type porous-sheets Stirling regenerator, Int J Therm Sci 94 (2015) 37–49.
[8] D.G. Thombare, S.K. Verma, Technological development in the Stirling cycle engines, Renew Sustain Energy Rev 12 (1) (2008) 1–38.
[9] J.R. Senft, Theoretical limits on the performance of stirling engines, Int J Energy Res 22 (11) (1998) 991–1000.
[10] I. Tlili, Y. Timoumi, S.B. Nasrallah, Thermodynamic analysis of the Stirling heat engine with regenerative losses and internal irreversibilities, Int J Engine Res 9 (1) (2008) 45–56.
[11] M. Costea, S. Petrescu, C. Harman, The effect of irreversibilities on solar Stirling engine cycle performance, Energy Convers Manag 40 (15–16) (1999) 1723–1731.
[12] S. Petrescu, M. Costea, C. Harman, T. Florea, Application of the Direct Method to irreversible Stirling cycles with finite speed, Int J Energy Res 26 (7) (2002) 589–609.
[13] F.L. Curzon, B. Ahlborn, Efficiency of a Carnot engine at maximum power output, Am J Phys 43 (1) (1975) 22–24.
[14] D.A. Blank, G.W. Davis, C. Wu, Power optimization of an endoreversible stirling cycle with regeneration, Energy 19 (1) (1994) 125–133.
[15] J.C. Chen, Z.J. Yan, L.X. Chen, B. Andresen, Efficiency bound of a solar-driven Stirling heat engine system, Int J Energy Res 22 (9) (1998) 805–812.
[16] F. Wu, L.G. Chen, C. Wu, F.G. Sun, Optimum performance of irreversible stirling engine with imperfect regeneration, Energy Convers Manag 39 (8) (1998) 727–732.
[17] S.C. Kaushik, S. Kumar, Finite time thermodynamic analysis of endoreversible Stirling heat engine with regenerative losses, Energy 25 (10) (2000) 989–1003.
[18] S.C. Kaushik, S. Kumar, Finite time thermodynamic evaluation of irreversible Ericsson and Stirling heat engines, Energy Convers Manag 42 (3) (2001) 295–312.
[19] S.C. Kaushik, S.K. Tyagi, S.K. Bose, M.K. Singhal, Performance evaluation of

irreversible Stirling and Ericsson heat pump cycles, Int J Therm Sci 41 (2) (2002) 193–200.
[20] M.H. Ahmadi, M.A. Ahmadi, M. Mehrpooya, Investigation of the effect of design parameters on power output and thermal efficiency of a Stirling engine by thermodynamic analysis, Int J Low-Carbon Technol 11 (2) (2016) 141–156.
[21] Y.Q. Li, Y.L. He, W.W. Wang, Optimization of solar-powered Stirling heat engine with finite-time thermodynamics, Renew Energy 36 (1) (2011) 421–427.
[22] S.K. Tyagi, J.C. Chen, S.C. Kaushik, Thermoeconomic optimization and parametric study of an irreversible Stirling heat pump cycle, Int J Therm Sci 43 (1) (2004) 105–112.
[23] F. Angulo-Brown, An ecological optimization criterion for finite-time heat engines, J Appl Phys 69 (11) (1991) 7465–7469.
[24] Z. Yan, Comment on An ecological optimization criterion for finite-time heat engines, J. Appl Phys 69 (7465) (1991)]. Journal Of Applied Physics. 1993;73(7):3583.
[25] R. Long, W. Liu, Ecological optimization for general heat engines, Phys A 434 (2015) 232–239.
[26] J. He, J. Chen, C. Wu, Ecological optimisation of an irreversible Stirling heat engine, Int J Ambient Energy 22 (4) (2001) 211–220.
[27] S.K. Tyagi, S.C. Kaushik, R. Salhotra, Ecological optimization and performance study of irreversible Stirling and Ericsson heat engines, J Phys D Appl Phys 35 (20) (2002) 2668–2675.
[28] M.H. Ahmadi, M.A. Ahmadi, Thermodynamic analysis and optimization of an irreversible Ericsson cryogenic refrigerator cycle, Energy Convers Manag 89 (2015) 147–155.
[29] M.H. Ahmadi, M.A. Ahmadi, Thermodynamic analysis and optimisation of an irreversible radiative-type heat engine by using non-dominated sorting genetic algorithm, Int J Ambient Energy 37 (4) (2016) 403–408.
[30] M.H. Ahmadi, M.A. Ahmadi, M. Mehrpooya, H. Hosseinzade, M. Feidt, Thermodynamic and thermo-economic analysis and optimization of performance of irreversible four-temperature-level absorption refrigeration, Energy Convers Manag 88 (2014) 1051–1059.
[31] R. Long, B. Li, Z. Liu, W. Liu, Performance analysis of a thermally regenerative electrochemical cycle for harvesting waste heat, Energy 87 (2015) 463–469.
[32] R. Long, B. Li, Z. Liu, W. Liu, Ecological analysis of a thermally regenerative electrochemical cycle, Energy 107 (2016) 95–102.
[33] Y. Ust, Ecological performance analysis and optimization of power generation systems, Ph. D., Thesis Progress Report Yildiz Technical University, Istanbul, 2004.
[34] M.H. Ahmadi, M.A. Ahmadi, M. Mehrpooya, M. Sameti, Thermo-ecological analysis and optimization performance of an irreversible three-heat-source absorption heat pump, Energy Convers Manag 90 (2015) 175–183.
[35] M.H. Ahmadi, M.A. Ahmadi, M. Feidt, Thermodynamic analysis and evolutionary algorithm based on multi-objective optimization of performance for irreversible four-temperature-level refrigeration, Mech Ind 16 (2) (2015) 207.
[36] M.H. Ahmadi, M.A. Ahmadi, M. Feidt, Performance optimization of a solar-driven multi-step irreversible brayton cycle based on a multi-objective genetic algorithm, Oil Gas Sci Technol 71 (1) (2016) 16.
[37] M.H. Ahmadi, M.A. Ahmadi, A. Shafaei, M. Ashouri, S. Toghyani, Thermodynamic analysis and optimization of the Atkinson engine by using NSGA-II, Int J Low-Carbon Technol 11 (3) (2016) 317–324.
[38] S.A. Sadatsakkak, M.H. Ahmadi, M.A. Ahmadi, Optimization performance and thermodynamic analysis of an irreversible nano scale Brayton cycle operating with Maxwell-Boltzmann gas, Energy Convers Manag 101 (2015) 592–605.
[39] S.A. Sadatsakkak, M.H. Ahmadi, M.A. Ahmadi, Thermodynamic and thermo-economic analysis and optimization of an irreversible regenerative closed Brayton cycle, Energy Convers Manag 94 (2015) 124–129.
[40] S. Toghyani, A. Kasaeian, M.H. Ahmadi, Multi-objective optimization of Stirling engine using non-ideal adiabatic method, Energy Convers Manag 80 (2014) 54–62.
[41] M.H. Ahmadi, M.A. Ahmadi, M. Mehrpooya, S.M. Pourkiaei, M. Khalili, Thermodynamic analysis and evolutionary algorithm based on multi-objective optimisation of the Rankine cycle heat engine, Int J Ambient Energy 37 (4) (2016) 363–371.
[42] M.H. Ahmadi, M.A. Ahmadi, S.A. Sadatsakkak, Thermodynamic analysis and performance optimization of irreversible Carnot refrigerator by using multi-objective evolutionary algorithms (MOEAs), Renew Sustain Energy Rev 51 (2015) 1055–1070.
[43] Z.Y. Luo, U. Sultan, M.J. Ni, H. Peng, B.W. Shi, G. Xiao, Multi-objective optimization for GPU3 Stirling engine by combining multi-objective algorithms, Renew Energy 94 (2016) 114–125.
[44] M.H. Ahmadi, H. Sayyaadi, S. Dehghani, H. Hosseinzade, Designing a solar powered Stirling heat engine based on multiple criteria: maximized thermal efficiency and power, Energy Convers Manag 75 (2013) 282–291.
[45] M.H. Ahmadi, H. Sayyaadi, H. Hosseinzadeh, Optimization of output power and thermal efficiency of solar-dish stirling engine using finite time thermodynamic analysis, Heat Transf-Asian Re 44 (4) (2015) 347–376.
[46] M.H. Ahmadi, H. Sayyaadi, A.H. Mohammadi, M.A. Barranco-Jimenez, Thermo-economic multi-objective optimization of solar dish-Stirling engine by implementing evolutionary algorithm, Energy Convers Manag 73 (2013) 370–380.
[47] M.H. Ahmadi, M.A. Ahmadi, A.H. Mohammadi, M. Mehrpooya, M. Feidt, Thermodynamic optimization of Stirling heat pump based on multiple criteria, Energy Convers Manag 80 (2014) 319–328.
[48] M.H. Ahmadi, M.A. Ahmadi, A. Mellit, F. Pourfayaz, M. Feidt, Thermodynamic analysis and multi objective optimization of performance of solar dish Stirling engine by the centrality of entransy and entropy generation, Int J Electr Power & Energy Syst 78 (2016) 88–95.
[49] M.H. Ahmadi, H. Hosseinzade, H. Sayyaadi, A.H. Mohammadi, F. Kimiaghalam, Application of the multi-objective optimization method for designing a powered Stirling heat engine: design with maximized power, thermal efficiency and minimized pressure loss, Renew Energy 60 (2013) 313–322.
[50] M.H. Ahmadi, M.A. Ahmadi, R. Bayat, M. Ashouri, M. Feidt, Thermo-economic optimization of Stirling heat pump by using non-dominated sorting genetic algorithm, Energy Convers Manag 91 (2015) 315–322.
[51] M.H. Ahmadi, M.A. Ahmadi, A.H. Mohammadi, M. Feidt, S.M. Pourkiaei, Multi-objective optimization of an irreversible Stirling cryogenic refrigerator cycle, Energy Convers Manag 82 (2014) 351–360.
[52] R. Long, B. Li, Z. Liu, W. Liu, Multi-objective optimization of a continuous thermally regenerative electrochemical cycle for waste heat recovery, Energy 93 (1) (2015) 1022–1029.
[53] J.E.R. Kennedy, Particle swarm optimization. Perth, Proc IEEE Int Conf Neural Netw (1995) 1995 1942-1948.
[54] C.A.C. Coello, G.T. Pulido, M.S. Lechuga, Handling multiple objectives with particle swarm optimization, Ieee T Evol Comput 8 (3) (2004) 256–279.
[55] C. Duan, X. Wang, S. Shu, C. Jing, H. Chang, Thermodynamic design of Stirling engine using multi-objective particle swarm optimization algorithm, Energy Convers Manag 84 (2014) 88–96.
[56] C.R. Raquel, P.C. Naval, An effective use of crowding distance in multiobjective particle swarm optimization, GECCO 2005: genetic and evolutionary computation conference, vols. 1 and 2, 2005, pp. 257–264.
[57] B. Zhou, X.T. Cheng, X.G. Liang, Power output analyses and optimizations of the Stirling cycle, Sci China-Technological Sci 56 (1) (2013) 228–236.